Asian Journal of Chemistry; Vol. 38, No. 9 (2026), 2427-2437
ASIAN JOURNAL OF CHEMISTRY
https://doi.org/10.14233/ajchem.2026.36490

Barleria acuminata Extract-Mediated Organic–Inorganic Copper Phosphate Nanohybrids: Synthesis, Optimization and Antioxidant Potential

R. PALASKAR[1], K. SHINDE[2], D. DHOKANE[1], M. NIMBALKAR[3], A. BELHEKAR[4] and U. JADHAV[1,*]

[1]Department of Microbiology, Savitribai Phule Pune University, Pune-411007, India
[2]Department of Biotechnology, Shivaji University, Kolhapur-416004, India
[3]Department of Botany, Shivaji University, Kolhapur-416004, India
[4]Department of Chemistry, Savitribai Phule Pune University, Pune-411007, India

*Corresponding author: E-mail: umeshjadhav02@gmail.com; ujadhav@unipune.ac.in

Received: 25 May 2026 *Accepted*: 13 August 2026 *Published online*: 5 September 2026 AJC-22471

In the present study, we report the green synthesis of *Barleria acuminata* extract mediated copper phosphate nanohybrids (BAE-CuPNHs) by a simple one-pot co-precipitation approach. Aqueous extracts of six different *Barleria* species were prepared by using ultrasonication and microwave-assisted extraction methods and evaluated for total phenolic content (TPC), total flavonoid content (TFC) and antioxidant activity. Among the tested species, *B. acuminata* showed highest phytochemical content and DPPH radical scavenging activity and was selected for nanohybrid preparation. The formation of nanohybrid was screened for different metal ions. Copper ions formed well-defined flower-like nanostructures with high efficiency of phytochemical immobilization. Optimization studies showed 4 mM $CuSO_4$, 2.0 mL PBS, static incubation and an incubation period of 72 h as the optimum conditions for the synthesis. FESEM, EDX, FTIR and XRD characterization confirmed the formation of crystalline BAE-CuPNHs with marigold-like morphology. The synthesized BAE-CuPNHs displayed antioxidant activity, indicating their promising prospects for antioxidant delivery and bioactive applications.

Keywords: *Barleria acuminata*, Organic-inorganic nanohybrid, Phytochemical immobilization, Antioxidant activity.

INTRODUCTION

Medicinal plants have long served as a rich reservoir of bioactive compounds with significant therapeutic potential [1,2]. Among these, species belonging to the genus *Barleria* (family Acanthaceae) have attracted increasing scientific attention due to their diverse phytochemical composition and broad spectrum of pharmacological activities. The genus *Barleria* comprises approximately 300 species distributed across tropical regions, with a notable diversity in India, where several species are endemic and traditionally used in folk medicine for the treatment of ailments such as cough, inflammation, diabetes and liver disorders. Phytochemical investigations have revealed that *Barleria* species are rich in bioactive constituents, including flavonoids, phenolics, iridoid glycosides, tannins and triterpenoids such as betulin, along with pharmacologically important alkaloids like vasicine and vasicinone. These compounds are well known for their potent antioxidant, anti-inflammatory, antimicrobial, hepatoprotective and anticancer activities [3,4].

The antioxidant potential of *Barleria* species is primarily attributed to their high total phenolic and flavonoid content, which play a crucial role in scavenging reactive oxygen species (ROS) and reducing oxidative stress. Comparative studies across multiple *Barleria* species have demonstrated significant variation in antioxidant activity. In addition to antioxidant assays such as DPPH, FRAP and ABTS, advanced analytical techniques like RP-HPLC have been employed to quantify key bioactive markers, providing deeper insight into their therapeutic potential and chemical diversity [5]. In recent years, there has been a growing emphasis on the exploration of natural antioxidants derived from plant sources due to their biocompatibility, low toxicity and diverse pharmacological properties. However, despite their potent bioactivity, plant-derived antioxidants often suffer from inherent limitations such as poor stability, low solubility, rapid degradation and limited bioavailability, which significantly hinder their effective utilization in therapeutic and industrial applications [6,7].

Despite their promising pharmacological properties, plant derived bioactive compounds often suffer from instability

under light, temperature, oxygen and pH variations, resulting in degradation and reduced bioavailability and efficacy. Nanotechnology offers an effective approach to improve the stability, bioavailability and controlled delivery of phytochemicals [8]. The organic-inorganic hybrid nanostructures are particularly attractive since they combine the properties of both components. Among these, nanoflower-like structures are hierarchical materials with flower-shaped morphology, high surface-to-volume ratio and loading capacity. They are generally formed through coordination between functional groups such as amine, hydroxyl and carboxyl groups and metal ions, including Cu^{2+} [9,10].

Hybrid nanoflowers were initially developed for enzyme immobilization and showed improved catalytic activity and stability compared with free enzymes [11]. Their application has since expanded to proteins, amino acids [12] and plant extracts [9]. Plant extracts provide a cost-effective, eco-friendly source of diverse functional groups for metal coordination and support green synthesis without toxic reagents or harsh conditions. Plant extract-mediated nanoflowers have also demonstrated enhanced antioxidant, antimicrobial and catalytic activities, attributed to the synergistic interaction between phytochemicals and the inorganic matrix, together with increased surface area and structural stability [13,14].

Although copper phosphate-based organic–inorganic nanohybrids have been prepared using proteins, enzymes, peptides and plant-derived molecules, the use of medicinal *Barleria* species as organic building blocks for copper phosphate hybrid nanostructures remains unexplored. Polyphenolic compounds can coordinate with Cu^{2+} through oxygen-containing functional groups to form hybrid nanoflowers [15]. The rich phenolic and flavonoid content and antioxidant potential of *Barleria* species therefore make them promising sources for developing antioxidant nanohybrids. However, comparative studies on the influence of different divalent metal ions on phytochemical-mediated hybrid formation and morphology remain limited. We hypothesized that both the phytochemical composition and metal-ion type would influence phytochemical immobilization and nanostructure formation.

Accordingly, six *Barleria* species were screened based on total phenolic content, total flavonoid content and antioxidant activity to identify the most suitable phytochemical source. The selected extract was then evaluated with different divalent metal ions to determine their effects on hybrid formation and morphology. The optimum plant-metal combination was further subjected to systematic optimization of synthesis conditions, followed by physico-chemical characterization and antioxidant evaluation. Unlike previous studies using a single plant extract and predefined metal precursor, this work employs a systematic screening strategy involving plant selection, metal ion selection and synthesis optimization. The study therefore provides a rational approach for developing plant-mediated organic–inorganic nanohybrids and establishes *Barleria acuminata* as a previously unexplored phytochemical source for copper phosphate-based hybrid nanostructures.

EXPERIMENTAL

The procured metal salts, absolute methanol, reagents for phosphate buffer saline (PBS), 2,2-diphenyl-1-picrylhydrazyl (DPPH) and ascorbic acid were of analytical grade.

Plant material collection and preparation: Fresh leaves of six *Barleria* sp. *i.e. B. cristata*, *B. terminalis*, *B. strigosa*, *B. grandiflora*, *B. acuminata* and *B. longifera* were obtained from the Botanical Garden, Kolhapur, India. The plant materials were washed thoroughly with distilled water, air-dried at room temperature and ground into a fine powder for extraction.

Preparation of aqueous plant extracts by ultrasonication and microwave-assisted extraction: Dried and finely powdered plant leaves of six *Barleria* species were used for the extraction of phytoconstituents. A 20% (w/v) aqueous extract was prepared by dispersing 20 g of leaf powder in 100 mL of distilled water, ensuring proper mixing to obtain a uniform suspension. For ultrasonication-assisted extraction (UAE), the prepared suspension was subjected to sonication in an ultrasonic bath operating at a frequency of 50 kHz for 30 min. Upon completion, the mixture was allowed to settle briefly and subsequently filtered through Whatman No. 1 filter paper to remove insoluble matter. The filtrate was collected and stored at 4 ºC in Amber-coloured containers until further use. In microwave-assisted extraction (MAE), 20 g of leaf powder was dispersed in 100 mL of distilled water and transferred to a microwave-compatible vessel and exposed to microwave irradiation for 1 min. After treatment, the mixture was allowed to cool to room temperature and then filtered using Whatman No. 1 filter paper. The resulting extract was collected and stored at 4 ºC for subsequent analysis. Both extraction methods were employed to facilitate efficient recovery of phytochemicals [16-18].

Phytochemical screening

Quantification of total phenolic content (TPC): The total phenolic content of the extracts was determined by the Folin-Ciocalteu method with some modifications [19]. The experiment was performed in 96 well microtitre to check total phenolic contents. A 50 µL of distilled water was added to each well, then 12.5 µL of plant extract and 12.5 µL of FC reagent was added. The reaction mixture was incubated for 10 min at room temperature. To this 125 µL Na_2CO_3 (7%) and 100 µL of distilled water were added and again incubated for 90 min in dark at 37 ºC. Absorbance was measured at 760 nm wavelength. Gallic acid solutions ranging from (20, 40, 60, 80 and 100 µg/mL) were used to construct the standard calibration curve ($y = 0.0061x + 0.05$, $R^2 = 0.9992$) and the total phenolic content was expressed as milligrams of gallic acid equivalents per gram of dry plant material (mg GAE/g).

Quantification of total flavonoid content (TFC): The content of total flavonoid in aqueous extract was assessed followed by Chang *et al.* [20]. For total flavonoid content determination, 150 µL of plant extract was mixed with 150 µL of 2% $AlCl_3$ solution and incubated in the dark for 10 min. The absorbance was measured at 367 nm. Quercetin solutions (20, 40, 60, 80 and 100 µg/mL) were used to construct the calibration curve, which showed a linear relationship ($y = 0.01x – 0.0896$, $R^2 = 0.9964$). The total flavonoid content was expressed as milligrams of quercetin equivalents per gram of dry plant material (mg QE/g).

DPPH radical scavenging assay: The antioxidant activity of the plant extracts was evaluated using the DPPH radical scavenging assay. Freshly prepared 0.1 mM DPPH solution

in ethanol (290 µL) was mixed with 10 µL of plant extract, shaken thoroughly and incubated in the dark at room temperature for 30 min. The absorbance was subsequently measured at 517 nm using a Shimadzu UV-1800 spectrophotometer [21,22].

Synthesis and screening of plant extract-metal ions based nanohybrid: Metal ion screening for nanohybrid formation was performed following a reported protocol with minor modifications [23]. Briefly, 50 mL of phosphate-buffered saline (PBS; 10 mM, pH 7.4) was mixed with 0.5 mL of plant extract (100 mg mL^{-1} stock solution). Subsequently, 1 mL of 200 mM aqueous solution of each metal salt [$CuSO_4·5H_2O$, $FeSO_4·7H_2O$, $MnSO_4·H_2O$, $CaCl_2·2H_2O$, $CoSO_4·7H_2O$, $MgSO_4·7H_2O$ and $ZnSO_4·7H_2O$], was added separately. The mixtures were agitated for 30 s to ensure uniform mixing and incubated statically at 4 ºC for three days. The resulting precipitates were collected by centrifugation at 10,000 rpm for 10 min at 4 ºC and dried in the dark at 4 °C to obtain the nanohybrid powders. An extract-free nanohybrid was prepared by mixing 1 mL of $CuSO_4$ with 50 mL of PBS (10 mM, pH 7.4). The antioxidant activity of the supernatants was evaluated using the DPPH radical-scavenging assay and expressed as percentage radical-scavenging activity (%RSA).

Determination of phytochemical immobilization efficiency: The immobilization efficiency of total phenolic content (TPC) and total flavonoid content (TFC) was determined by comparing the phytochemical content of the initial extract with that remaining in the supernatant after nanohybrid synthesis. The immobilization efficiency (%) was calculated using the following equations:

$$\text{Immobilization efficiency (\%)} = \frac{TPC_{initial} - TPC_{supernatant}}{TPC_{initial}} \times 100$$

Similarly,

$$\text{Immobilization efficiency (\%)} = \frac{TFC_{initial} - TFC_{supernatant}}{TFC_{initial}} \times 100$$

where $TPC_{initial}$ = total phenolic content of the initial plant extract before immobilization; $TPC_{supernatant}$ = total phenolic content remaining in the supernatant after nanohybrid formation; $TFC_{initial}$ = total flavonoid content of the initial plant extract before immobilization; $TFC_{supernatant}$ = total flavonoid content remaining in the supernatant after nanohybrid formation.

Optimization study: A one-factor-at-a-time (OFAT) approach was used to optimize the synthesis of *B. acuminata* extract-mediated copper phosphate nanohybrids (BAE-CuPNHs). Four synthesis variables, *viz*. $CuSO_4$ concentration (1-5 mM), PBS volume (0.5-2.5 mL), incubation condition (static or shaking) and incubation period (24-72 h), were systematically varied while keeping the remaining parameters constant. Following incubation, the reaction mixtures were centrifuged to separate the nanohybrid fraction and the supernatants were collected for further analysis. The antioxidant activity of the supernatants was evaluated using the DPPH radical-scavenging assay. A decrease in supernatant antioxidant activity was considered an indirect indication of the interaction and immobilization of antioxidant phytoconstituents within the copper-based nanohybrid matrix. Thus, the condition producing the lowest residual antioxidant activity was selected as optimal [23,24].

After optimization, the antioxidant activity of BAE-CuPNHs was evaluated using the DPPH radical-scavenging assay with slight modifications. Briefly, BAE-CuPNHs (1-5 mg) were reacted with freshly prepared DPPH solution and incubated at room temperature in the dark. The mixtures were then centrifuged to remove the nanohybrid particles and the clear supernatants were collected. Absorbance was measured at 517 nm using a UV-Visible spectrophotometer. A DPPH solution without the sample was used as the control and the percentage radical-scavenging activity was calculated using the above equation [21,22].

Characterization: Surface morphology was examined by field-emission scanning electron microscopy (FESEM; FET Nova NanoSEM 450), while elemental composition was determined by energy-dispersive X-ray spectroscopy (EDX). The functional groups and phytochemical interactions were analyzed by Fourier-transform infrared spectroscopy (FTIR; Shimadzu FTIR-8900) over 4500-450 cm^{-1}. The crystal structure was determined by X-ray diffraction (XRD) analysis.

Statistical analysis: All experiments were performed in triplicate (n = 3) and the results were expressed as mean ± standard deviation (SD). Statistical analyses were carried out using OriginPro 2020. Differences among experimental groups were evaluated using one-way analysis of variance (ANOVA), followed by Tukey's honestly significant difference (HSD) post hoc multiple comparison test for pairwise comparisons. ANOVA results are reported as F-values, degrees of freedom (df) and exact *p*-values, while statistically significant pairwise differences identified by Tukey's HSD test were also reported. Differences were considered statistically significant at $p < 0.05$.

RESULTS AND DISCUSSION

Primary quantitative analysis of phytoconstituents: Aqueous extraction of phytoconstituents from *Barleria* leaves was successfully performed using ultrasonication-assisted extraction (UAE) and microwave-assisted extraction (MAE). Both methods produced clear, homogeneous 20% (w/v) extracts after filtration. UAE (50 kHz, 30 min) and MAE (1 min) effectively released water-soluble phytochemicals, with MAE providing comparable extraction efficiency in a substantially shorter time.

Extraction method and plant species significantly affected the recovery of phenolic and flavonoid compounds (Table-1). One-way ANOVA confirmed significant differences in total phenolic content (TPC) and total flavonoid content (TFC) among the six *Barleria* species for both UAE and MAE ($p < 0.001$).

For UAE extracts, TPC differed significantly among species ($F(5,12) = 130.40$, $p = 4.99 \times 10^{-10}$). *B. longifera* exhibited the highest TPC (1.004 ± 0.020 mg GAE/g dry plant material), followed by *B. acuminata* (0.873 ± 0.040 mg GAE/g dry plant material), whereas *B. strigosa* showed the lowest phenolic content (0.491 ± 0.024 mg GAE/g dry plant material). Tukey's HSD test indicated that *B. longifera* possessed significantly higher TPC than most of the remaining

TABLE-1
TOTAL PHENOLIC CONTENT (TPC) AND TOTAL FLAVONOID CONTENT (TFC) OF *Barleria* SPECIES EXTRACTED BY ULTRASONICATION-ASSISTED EXTRACTION (UAE) AND MICROWAVE-ASSISTED EXTRACTION (MAE)

Sample	TPC (mg GAE/g dry plant material)		TFC (mg QE/g dry plant material)	
	Sonication	Microwave	Sonication	Microwave
B. cristata	0.798 ± 0.049^{b}	0.765 ± 0.003^{c}	0.924 ± 0.008^{c}	0.420 ± 0.059^{c}
B. terminalis	0.690 ± 0.008^{c}	0.675 ± 0.015^{c}	0.975 ± 0.007^{b}	0.678 ± 0.031^{b}
B. grandiflora	0.554 ± 0.014^{d}	0.915 ± 0.021^{bc}	1.368 ± 0.023^{a}	0.531 ± 0.009^{c}
B. strigosa	0.491 ± 0.024^{d}	1.112 ± 0.579^{ab}	0.925 ± 0.009^{c}	0.730 ± 0.007^{b}
B. acuminata	0.873 ± 0.040^{ab}	2.395 ± 0.013^{a}	1.484 ± 0.004^{c}	1.003 ± 0.040^{a}
B. longifera	1.004 ± 0.020^{a}	2.095 ± 0.442^{ab}	0.917 ± 0.002^{c}	0.643 ± 0.032^{b}

Footnote: Values are presented as mean ± standard deviation (n = 3). Means within the same column followed by different lowercase superscript letters are significantly different according to Tukey's honestly significant difference (HSD) multiple comparison test at $p < 0.05$ following one-way ANOVA. Means sharing at least one common letter are not significantly different ($p > 0.05$).

species, while no significant difference was observed between *B. acuminata* and *B. cristata* or between *B. grandiflora* and *B. strigosa* ($p > 0.05$).

In contrast, TPC of MAE extracts also varied significantly among species ($F(5,12) = 13.56$, $p = 0.00011$). *B. acuminata* exhibited the highest phenolic content (2.395 ± 0.013 mg GAE/g dry plant material), followed by *B. longifera* (2.095 ± 0.442 mg GAE/g dry plant material), whereas *B. terminalis* contained the lowest TPC (0.675 ± 0.015 mg GAE/g dry plant material). Tukey's HSD analysis showed that *B. acuminata* possessed significantly higher TPC than most other species, while no significant difference was observed between *B. acuminata* and *B. longifera*.

A similar trend was observed for flavonoid content. The TFC of UAE extracts differed significantly among the six *Barleria* species ($F(5,12) = 1492.9$, $p < 0.0001$). *B. acuminata* had the highest TFC (1.484 ± 0.004 mg QE/g), followed by *B. grandiflora* (1.368 ± 0.023 mg QE/g), while *B. longifera* had the lowest value (0.917 ± 0.002 mg QE/g). Tukey's HSD test placed *B. acuminata* and *B. grandiflora* significantly above the other species, while *B. cristata*, *B. strigosa* and *B. longifera* showed no significant difference.

For MAE extracts, TFC varied significantly among species ($F(5,12) = 68.96$, $p < 0.0001$). *B. acuminata* had the highest TFC (1.003 ± 0.040 mg QE/g), followed by *B. strigosa* (0.730 ± 0.007 mg QE/g) and *B. cristata* had the lowest (0.420 ± 0.059 mg QE/g). Tukey's HSD test showed significantly higher TFC for *B. acuminata* than the other species ($p < 0.05$), while *B. strigosa*, *B. terminalis* and *B. longifera* did not differ significantly.

MAE method provide higher phenolic recovery, particularly for *B. acuminata* and B. *longifera*, whereas UAE gave higher flavonoid recovery. *B. acuminata* had the highest flavonoid content and antioxidant activity under both extraction conditions (Fig. 1) and was selected for subsequent nanohybrid synthesis and optimization. These results agreed with previous reports of substantial variation in phenolic and flavonoid composition among *Barleria* species [25,26]. The

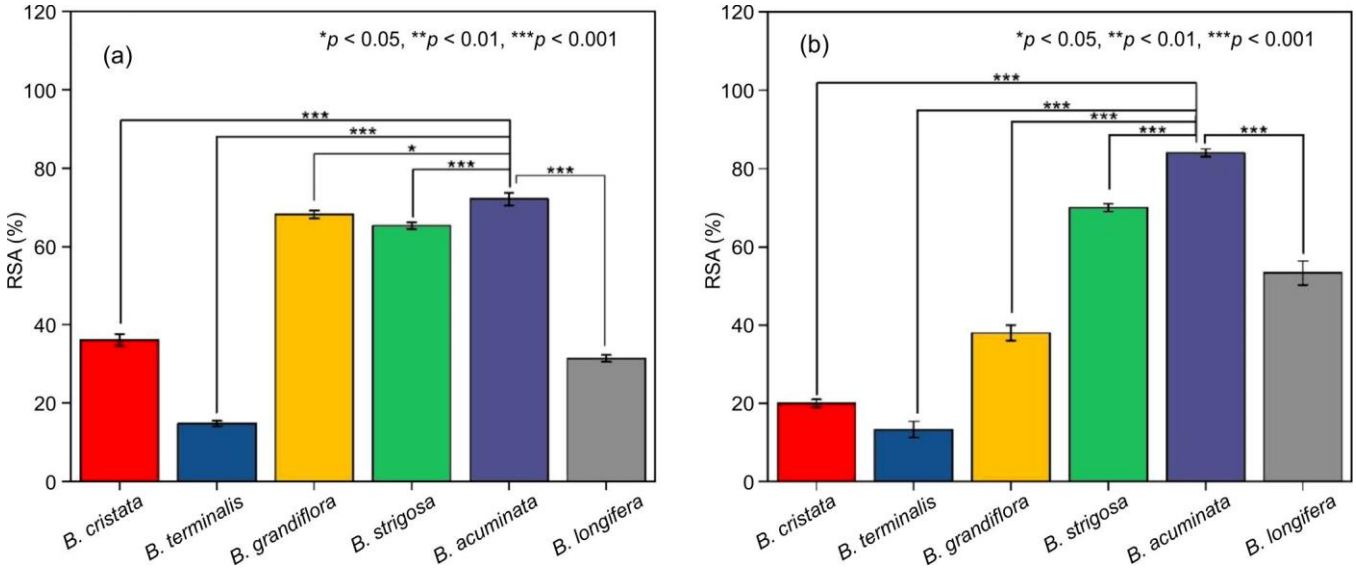

Fig. 1. DPPH radical scavenging activity (%) of aqueous extracts prepared by (a) ultrasonication-assisted extraction (UAE) and (b) microwave-assisted extraction (MAE) from six *Barleria* species. Values are presented as mean ± standard deviation (SD) (n = 3). Statistical analysis was performed using one-way ANOVA followed by Tukey's honestly significant difference (HSD) multiple comparison test. Asterisks indicate statistically significant differences between the compared groups ($p < 0.05$, $p < 0.01$, $p < 0.001$, $p < 0.0001$; ns = not significant)

higher phytochemical content and antioxidant activity of *B. acuminata* support its selection as the phytochemical source for antioxidant organic–inorganic nanohybrid synthesis.

Antioxidant activity: The DPPH radical-scavenging assay was used to evaluate the antioxidant activity of the UAE (Fig. 1a) and MAE (Fig. 1b) extracts. Significant differences were observed among the six Barleria species for both extraction methods. For UAE, one-way ANOVA showed a significant difference among species ($F(5,12) = 1306.54$, $p = 5.56 \times 10^{-16}$), with Tukey's HSD confirming significant differences ($p < 0.05$). *B. acuminata* showed the highest scavenging activity (72.11 ± 1.61%), followed by *B. grandiflora* (68.17 ± 1.00%), *B. strigosa* (65.34 ± 0.85%), *B. cristata* (36.15 ± 1.50%), *B. longifera* (31.41 ± 0.85%) and *B. terminalis* (14.84 ± 0.66%).

MAE extracts showed a similar species-dependent variation ($F(5,12) = 675.82$, $p = 2.87 \times 10^{-14}$). *B. acuminata* had the highest activity (84.00 ± 1.00%), followed by *B. strigosa* (70.00 ± 1.00%), *B. longifera* (53.33 ± 3.06%), *B.* grandiflora (38.00 ± 2.00%), *B. cristata* (20.00 ± 1.00%) and *B. terminalis* (13.33 ± 2.08%). Tukey's HSD confirmed significant differences among the species ($p < 0.05$).

B. acuminata exhibited the highest DPPH scavenging activity with both extraction methods and was selected for subsequent nanohybrid synthesis. MAE gave higher antioxidant activity than UAE for *B. acuminata* and several other species, consistent with reports attributing improved antioxidant recovery to microwave-assisted cell disruption [27]. The higher activity of *B. acuminata* was consistent with its higher phenolic content, supporting its selection as the phytochemical source for antioxidant nanohybrid fabrication.

Metal-ion screening and optimization of BAE-CuPNHs: The present study developed plant-mediated organic–inorganic nanohybrids using *B. acuminata* leaves extract as the organic component and a metal phosphate framework as the inorganic component. Formation of such hybrid structures generally involves interactions between metal ions and functional groups present in organic molecules, followed by self-assembly within the inorganic framework [28]. Hybrid nanoflower formation has been anticipated to involve nucleation followed by anisotropic crystal growth. During the initial stage, metal ions react with phosphate ions present in phosphate-buffered saline (PBS), forming metal phosphate nuclei. These nuclei can subsequently serve as sites for the association of organic molecules during crystal growth and hierarchical assembly [29-31]. Although the molecular interactions involved in the present system were not directly investigated, hydroxyl, carbonyl and other oxygen-containing functional groups present in *B. acuminata* phytochemicals may interact with the developing metal phosphate framework.

Different divalent metal ions were screened to identify a suitable inorganic precursor for nanohybrid formation. The screening was based on residual antioxidant activity in the synthesis supernatant and the morphology of the resulting materials observed by FESEM (Figs. 2 and 3). Residual TPC and TFC were subsequently quantified under optimized conditions as comparative measures of phytochemical immobilization. The metal-ion screening revealed clear differences in both residual antioxidant activity and nanostructure morphology.

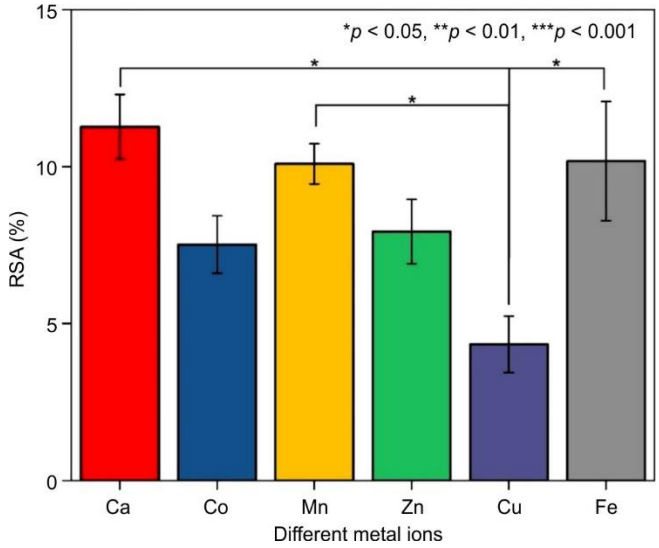

Fig. 2. Residual DPPH radical scavenging activity (%RSA) of the supernatants following nanohybrid synthesis using different divalent metal ions. Values are presented as mean ± standard deviation (SD) (n = 3). Statistical analysis was performed using one-way ANOVA followed by Tukey's honestly significant difference (HSD) multiple comparison test. Asterisks indicate statistically significant differences between the compared groups ($p < 0.05$, $p < 0.01$, $p < 0.001$, $p < 0.0001$; ns = not significant)

Calcium- and manganese-based systems retained relatively higher antioxidant activity in the supernatant and formed irregular, fragmented or granular structures. The ferrous ion system generated heterogeneous agglomerated particles with non-uniform morphology. The cobalt-based system showed a higher reduction in residual antioxidant activity and formed partially organized sheet-like and petal-like structures. Zinc- and copper-based systems exhibited the lowest residual antioxidant activity, accompanied by the formation of more organized hierarchical structures. Zinc generated compact spherical assemblies composed of densely packed nanosheets, whereas copper produced uniform flower-like structures consisting of interconnected petal-like features.

The residual antioxidant activity differed significantly among the metal-ion systems according to one-way ANOVA ($F(5,12) = 4.88$, $p = 0.0115$). Tukey's HSD test showed significantly lower residual activity for the copper-based system compared with calcium ($p = 0.0101$), iron ($p = 0.0320$) and manganese ($p = 0.0349$). The copper system had the lowest residual antioxidant activity (4.34 ± 1.55%), while calcium, iron and manganese retained 11.27 ± 1.79%, 10.17 ± 3.28% and 10.09 ± 1.11%, respectively. These results, together with the well-defined flower-like morphology observed by FESEM, supported the selection of Cu^{2+} as the inorganic precursor for subsequent studies. The suitability of Cu^{2+} for hybrid nanoflower formation is consistent with earlier reports [32,33]. The present study differs from approaches in which copper is selected before screening, as both phytochemical immobilization and nanostructural morphology were considered in the precursor selection.

Optimization of synthesis conditions: The synthesis of BAE-CuPNHs was optimized by monitoring residual antioxidant activity in the reaction supernatant (Fig. 4). A lower residual activity was used as an indirect measure of higher

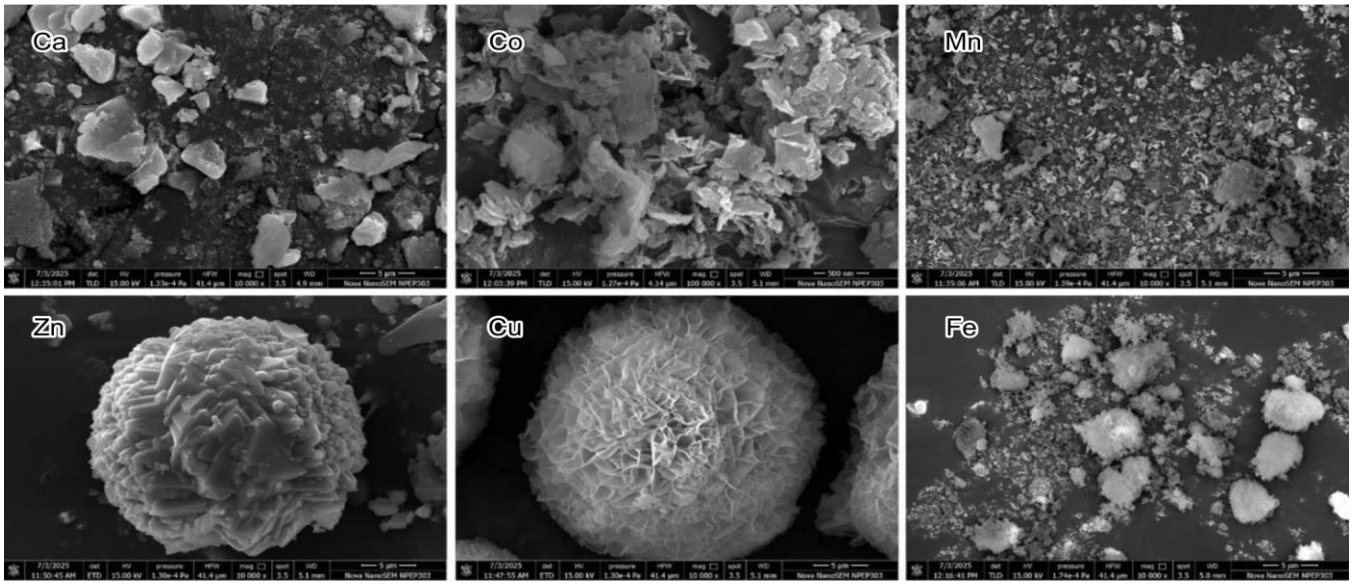

Fig. 3. FESEM images of different nanohybrid synthesized using different metal ions

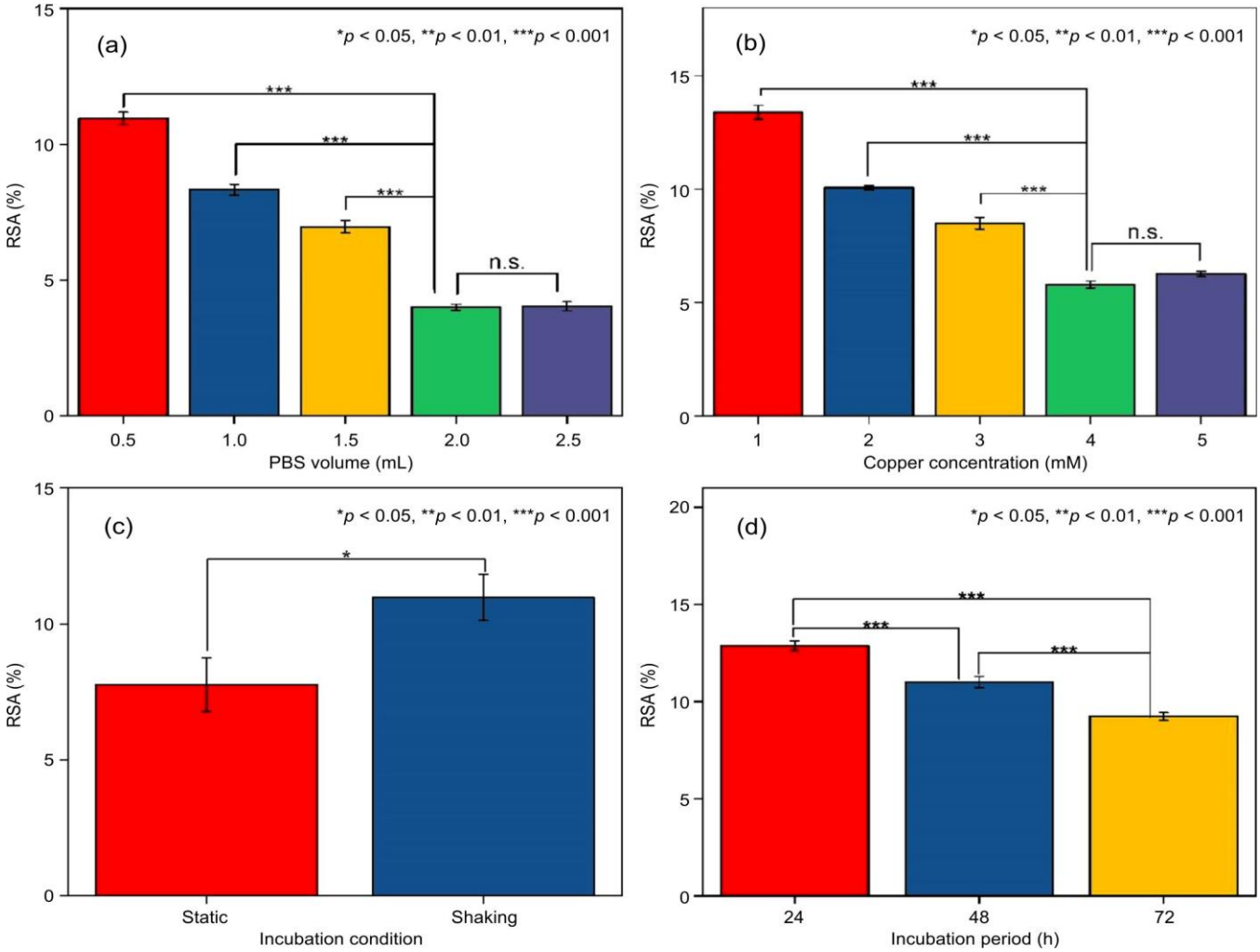

Fig. 4. Optimization of synthesis parameters for *Barleria acuminata* extract-mediated copper phosphate nanohybrids (BAE-CuPNHs): (a) effect of PBS volume, (b) effect of $CuSO_4$ concentration, (c) effect of incubation condition and (d) effect of incubation period. Values are presented as mean ± standard deviation (SD) (n = 3). Statistical analysis was performed using one-way ANOVA followed by Tukey's honestly significant difference (HSD) multiple comparison test. Asterisks indicate statistically significant differences between the compared groups ($p < 0.05$, $p < 0.01$, $p < 0.001$, $p < 0.0001$; ns = not significant)

immobilization of antioxidant phytochemicals within the nanohybrid matrix. Quantitative analysis of residual TPC and TFC under the selected conditions provided an additional assessment of phytochemical incorporation.

PBS volume had a significant effect on residual antioxidant activity ($F(4,10) = 717.81$, $p = 3.01 \times 10^{-12}$). Increasing the PBS volume from 0.5 to 2.0 mL progressively decreased residual activity, with Tukey's HSD showing significant differences between the tested volumes up to 2.0 mL ($p < 0.001$). The residual activity at 2.0 mL (4.00 ± 0.11%) was statistically comparable with that at 2.5 mL (4.04 ± 0.17%; adjusted $p = 0.9992$). Thus, 2.0 mL volume was selected as the optimum condition, as the higher volume did not provide a measurable improvement. The effect may be related to phosphate availability during copper phosphate framework formation.

Cu^{2+} concentration significantly affected the synthesis response ($F(4,10) = 229.02$, $p = 8.73 \times 10^{-10}$). Residual antioxidant activity decreased as Cu^{2+} concentration increased from 1 to 4 mM (Fig. 4b). Tukey's HSD test showed significant differences among the concentrations ($p < 0.05$), except between 4 and 5 mM ($p = 0.521$). The lowest residual activity was observed at 4 mM (5.80 ± 0.26%), while 5 mM gave a comparable value of 6.27 ± 0.21%. A concentration of 4 mM Cu^{2+} was selected, providing high phytochemical immobilization without the need for excess metal ions.

Incubation condition significantly influenced phytochemical immobilization ($F(1,4) = 18.68$, $p = 0.0124$). Static incubation resulted in lower residual antioxidant activity (7.77 ± 0.99%) than shaking incubation (10.97 ± 0.85%). Tukey's HSD confirmed a significant difference between the two conditions ($p = 0.0124$; Fig. 4c). The static incubation was selected for subsequent synthesis, as reduced mechanical disturbance may favour stable association between phytochemicals and the developing copper phosphate framework.

Incubation time also had a significant effect on residual antioxidant activity ($F(2,6) = 151.07$, $p = 7.38 \times 10^{-6}$). The residual activity decreased from 12.87 ± 0.25% at 24 h to 11.00 ± 0.30% at 48 h and 9.23 ± 0.21% at 72 h (Fig. 4d). Tukey's HSD showed significant differences among all incubation periods ($p < 0.05$). The 72 h period was selected, as extended incubation allowed better and higher association of phytochemicals with the developing nanohybrid matrix.

The optimized synthesis conditions were therefore 2.0 mL PBS, 4 mM Cu^{2+}, static incubation and 72 h reaction time. Earlier work on SBP-$Cu_3(PO_4)\cdot 3H_2O$ nanohybrids reported that phosphate ions from PBS participate in formation of the inorganic flower-like framework and identified 2 mM $CuSO_4$ in 5 mM PBS (pH 7.4) as suitable for hierarchical nanoflower formation [23]. The present results support the role of phosphate availability and copper concentration in nanohybrid formation while identifying conditions suitable for phytochemical immobilization from *B. acuminata* extract. BAE-CuPNHs prepared under these conditions were subjected to physico-chemical characterization and antioxidant evaluation.

Phytochemical immobilization: TPC and TFC were quantified in the initial *B. acuminata* extract and synthesis supernatant to assess phytochemical immobilization (Table-2). The initial TPC was 0.048525 ± 0.002 mg GAE/mL, which decreased to 0.003552 ± 0.001 mg GAE/mL after nanohybrid formation. This corresponded to an immobilization efficiency of 92.70 ± 0.70%. The TFC decreased from 0.15206 ± 0.010 mg QE/mL in the initial extract to 0.029493 ± 0.001 mg QE/mL in the supernatant, providing an immobilization efficiency of 80.58 ± 0.63%.

One-way ANOVA confirmed significant differences between the initial extract and supernatant for both TPC ($F(1,4) = 605.16$, $p < 0.0001$) and TFC ($F(1,4) = 451.52$, $p < 0.0001$). Tukey's HSD test confirmed significantly higher TPC and TFC in the initial extract than in the post-synthesis supernatant ($p < 0.001$). The substantial reduction in both phytochemical groups supports their incorporation into the nanohybrid during synthesis. Phenolic compounds showed a higher immobilization efficiency than flavonoids, which suggest stronger association of phenolic constituents with the copper phosphate matrix.

Based on the combined results from metal-ion screening, the synthesis optimization and phytochemical quantification establish Cu^{2+} as the preferred inorganic precursor and *B. acuminata* as a suitable phytochemical source for BAE-CuPNH fabrication. The optimized system showed high phenolic and flavonoid immobilization with well-defined hierarchical nanoflower structures.

Characterization of nanohybrid: The XRD analysis was performed to investigate the crystalline structure of the synthesized BAE-CuPNHs. The diffraction pattern was recorded using Cu*K*α radiation (λ = 0.15406 nm) over a 2θ range of 3-80º (Fig. 5). The synthesized material showed well-defined diffraction peaks with a crystalline structure. The diffraction pattern was consistent with JCPDS No. 00-022-0548 for $Cu_3(PO_4)_2\cdot 3H_2O$, while no peaks associated with secondary crystalline phases were detected.

The average crystallite size was estimated using the Debye-Scherrer equation:

$$D = \frac{k\lambda}{\beta \cos\theta}$$

where D is the crystallite size, k is the Scherrer constant (0.9), λ is the X-ray wavelength (0.15406 nm); β is the full-width at half maximum (FWHM) and θ is the Bragg angle. The copper

TABLE-2
TOTAL PHENOLIC CONTENT, TOTAL FLAVONOID CONTENT, ANTIOXIDANT ACTIVITY AND IMMOBILIZATION EFFICIENCY OF *B. acuminata* EXTRACT BEFORE AND AFTER NANOHYBRID SYNTHESIS

Parameter	Initial extract	Supernatant	Immobilization efficiency (%)
Total phenolic content (mg GAE/mL)	0.048525 ± 0.002	0.003552 ± 0.001	92.7 ± 0.70
Total flavonoid content (mg QE/mL)	0.15206 ± 0.010	0.029493 ± 0.001	80.58 ± 0.63
Antioxidant activity (% RSA)	30.66 ± 4.04	5.66 ± 1.52	81.54 ± 6.50

Values are expressed as mean ± SD (n = 3).

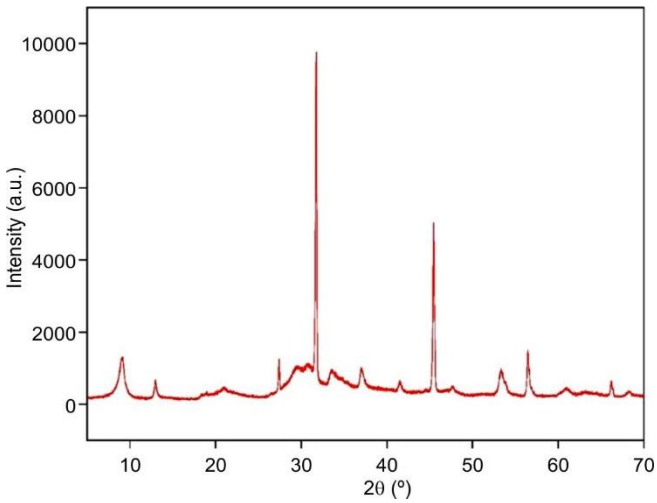

Fig. 5. XRD spectra of BAE-CuPNHs

phosphate domains exhibited an average crystallite size of ~40.5 nm based on XRD analysis.

FESEM analysis (Fig. 6) revealed well-defined flower-like structures composed of densely packed petal-like nanosheets radiating from the centre, with an average diameter of approximately 13 μm (Fig. 6b). The copper phosphate control exhibited a compact, wrinkled sheet-like morphology (Fig. 6a), whereas the presence of *B. acuminata* extract favoured hierarchical nanoflower formation. Comparable copper phosphate nanoflower morphologies have been reported for plant- and peptide-mediated hybrid systems [33]. The hierarchical architecture may provide a large accessible surface area for functional applications.

EDX analysis and elemental mapping (Fig. 7) confirmed the presence of C, O, P and Cu, consistent with the organic–inorganic composition of the nanohybrid. The elemental composition was Cu (19.68 wt.%), C (17.62 wt.%), O (10.17

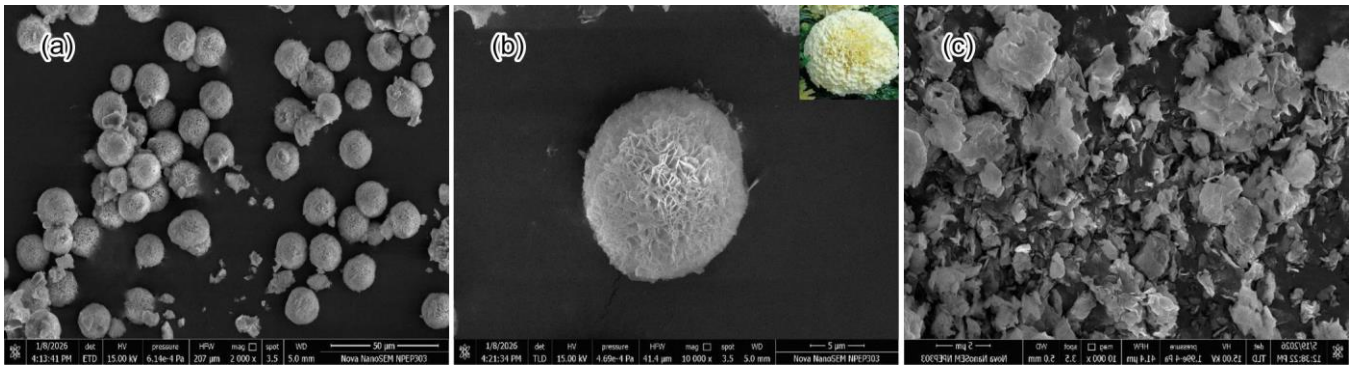

Fig. 6. FESEM images of BAE-CuPNHs (a) evenly distributed, (b) single nanoflower similar to that of natural marigold flowers, (c) $Cu_3(PO_4)_2$ crystals

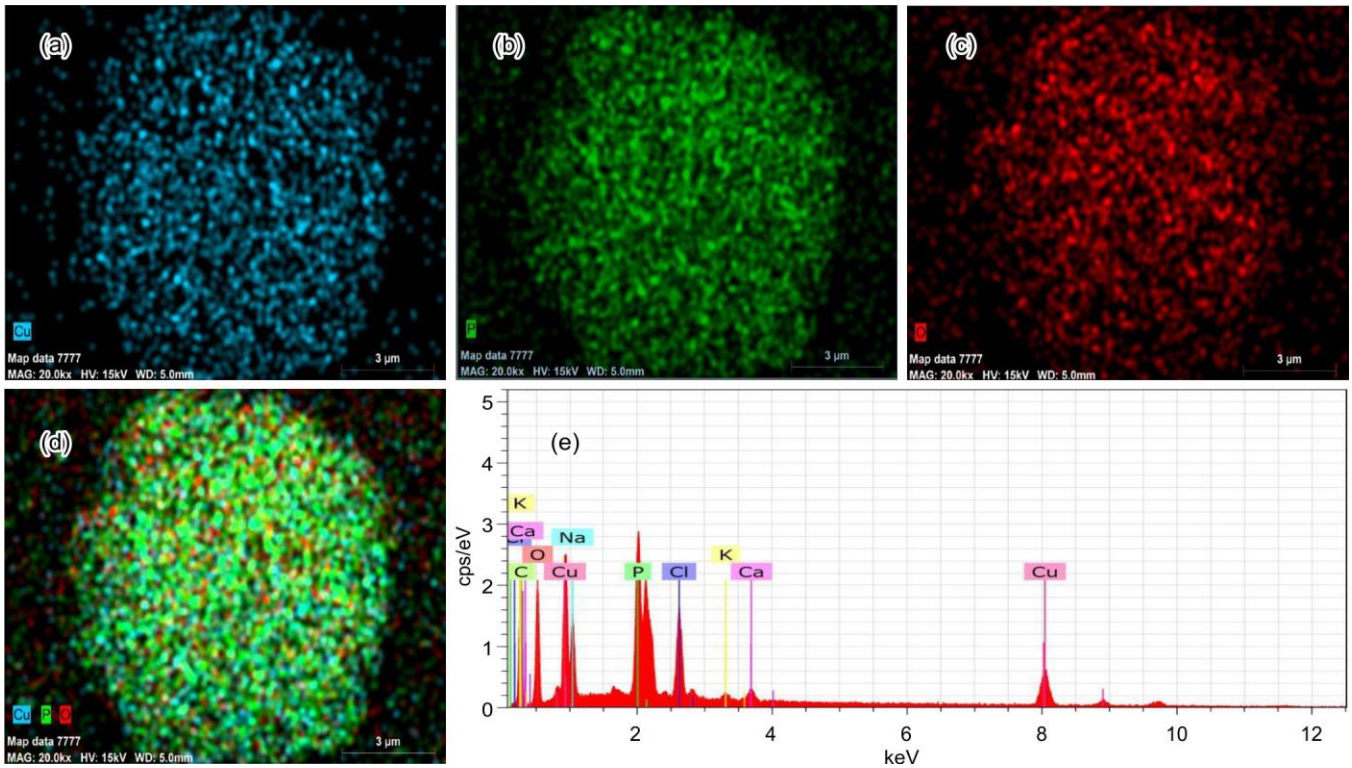

Fig. 7. EDX mapping & elemental analysis of BAE-CuPNHs

wt.%) and P (7.65 wt.%), with trace amounts of Na, Cl, Ca and K (Fig. 7e). Carbon and oxygen are associated mainly with plant-derived constituents, while copper and phosphorus correspond to the inorganic phase. Elemental mapping showed a relatively uniform distribution of Cu, P and O across the nanohybrid surface (Fig. 7a-d). The combined FESEM, EDX and XRD findings support the formation of a copper phosphate-based hierarchical nanohybrid.

FTIR spectroscopy was used to examine the functional groups of copper phosphate, *B. acuminata* extract and BAE-CuPNHs (Fig. 8). The BAE-CuPNH spectrum (Fig. 8a) retained characteristic bands of both components. The broad band at 3481.44 cm^{-1}, carbonyl band at 1739.34 cm^{-1} and bands at 1367.57 and 1216.07 cm^{-1} support the presence of plant derived constituents. Phosphate bands at 1149.02, 1044.88, and 989.23 cm^{-1}, along with deformation bands at 629.53, 559.08, 535.81 and 513.54 cm^{-1}, are the characteristic of the copper phosphate phase. The copper phosphate spectrum (Fig. 8b) showed phosphate bands at 1140.85, 1042.17 and 983.08 cm^{-1}, assigned to PO_4^{3-} asymmetric stretching, while bands at 623.35 and 552.68 cm^{-1} corresponded to O–P–O bending vibrations, which is the characteristic of the copper phosphate framework [34]. The *B. acuminata* extract (Fig. 8c) exhibited bands associated with plant-derived phytochemicals. The bands at 2925.71 and 2852.05 cm^{-1} were assigned to O–H and C–H stretching vibrations, respectively. The band at 1739.43 cm^{-1} corresponded to C=O stretching, while bands at 1367.24, 1261.02 and 1061.89 cm^{-1} were associated with O–H bending, C–O stretching and C–N stretching vibrations, respectively.

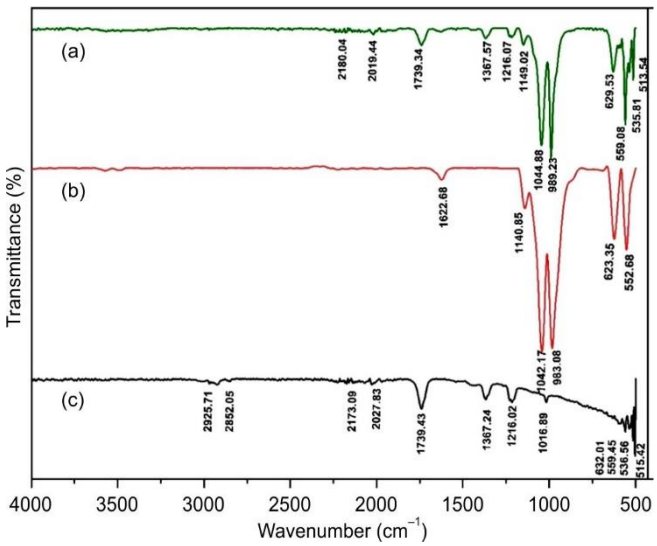

Fig. 8. FTIR analysis of the (a) BAE-CuPNHs, (b) copper phosphate and (c) *B. acuminata* extract

The small FTIR band shifts did not provide sufficient evidence for specific strong chemical interactions. The characteristic bands of copper phosphate and plant-derived constituents support their coexistence in the hybrid material, in agreement with the quantitative phytochemical immobilization results. Under optimized conditions, the immobilization efficiencies were 92.70 ± 0.70% for total phenolics and 80.58 ± 0.63% for total flavonoids (Table-2). Antioxidant activity showed an immobilization efficiency of 81.54 ± 6.5%. The antioxidant response decreased from 30.66 ± 4.04% RSA in the initial extract to 5.66 ± 1.52% RSA after nanohybrid formation. One-way ANOVA confirmed a significant difference between the two groups ($F(1,4) = 100.45$, $p < 0.0001$), and Tukey's test confirmed the lower final antioxidant activity ($p < 0.001$). These results provide quantitative support for substantial incorporation of antioxidant phytochemicals into the copper phosphate nanohybrid

Antioxidant activity: The antioxidant activity of BAE-CuPNHs was evaluated using the DPPH radical-scavenging assay (Fig. 9). A concentration-dependent increase in radical scavenging activity (%RSA) was observed. One-way ANOVA confirmed significant differences among the tested concentrations ($F(4,10) = 992.82$, $p = 5.99 \times 10^{-13}$), while Tukey's HSD test showed significant differences between all concentrations ($p < 0.001$). The %RSA increased from 39.00 ± 0.50% at 1 mg to 79.00 ± 0.50% at 5 mg, with intermediate values of 47.00 ± 1.53%, 56.33 ± 0.89% and 68.00 ± 0.50% at 2, 3 and 4 mg, respectively.

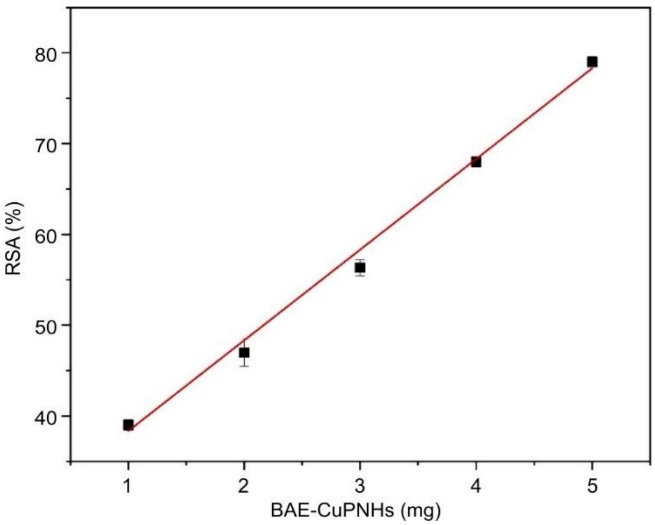

Fig. 9. DPPH radical scavenging activity of *Barleria acuminata* extract-mediated copper phosphate nanohybrids (BAE-CuPNHs) at different nanohybrid concentrations (1-5 mg). Values are presented as mean ± standard deviation (SD) (n = 3). Statistical analysis was performed using one-way ANOVA followed by Tukey's honestly significant difference (HSD) multiple comparison test. Asterisks indicate statistically significant differences between the compared groups ($p < 0.05$, $p < 0.01$, $p < 0.001$, $p < 0.0001$)

Linear regression showed a strong positive relationship between nanohybrid concentration and %RSA ($y = 28.36765 + 9.98529x$; $r = 0.99834$). The IC_{50} calculated from this regression was approximately 2.17 mg. The concentration dependent DPPH response indicates retention of antioxidant activity by immobilized phytochemicals within the copper phosphate matrix. The high immobilization efficiencies of phenolics, flavonoids and antioxidant constituents further demonstrate the preservation of phytochemical functionality. Similar concentration-dependent DPPH activity was reported for Cu-based organic–inorganic hybrid nanoflowers prepared using snakeskin shed [31]. The BAE-CuPNHs showed comparable radical-scavenging behaviour, highlighting their potential as plant-mediated antioxidant nanohybrids.

Conclusion

Aqueous phytochemical extraction from six *Barleria* species was evaluated using ultrasonication-assisted extraction (UAE) and microwave-assisted extraction (MAE). *B. acuminata* exhibited the highest DPPH radical-scavenging activity under both extraction conditions and was selected as the phytochemical source for nanohybrid synthesis. MAE provided higher phenolic recovery for *B. acuminata*, while UAE gave higher flavonoid recovery. Copper was selected from the screened divalent metal ions based on its low residual antioxidant activity and formation of well-defined hierarchical flower-like structures. The optimized synthesis conditions comprised 2.0 mL PBS, 4 mM $CuSO_4$, static incubation and 72 h reaction time. Under these conditions, BAE-CuPNHs achieved immobilization efficiencies of 92.70 ± 0.70% for phenolics, 80.58 ± 0.63% for flavonoids and 81.54 ± 6.5% for antioxidant constituents. XRD analysis assigned the crystalline phase to $Cu_3(PO_4)_2 \cdot 3H_2O$, with an average crystallite size of ~40.5 nm. FESEM revealed hierarchical nanoflowers composed of densely packed petal-like nanosheets, while EDX and FTIR analyses established the coexistence of copper phosphate and plant-derived constituents within the hybrid structure. The DPPH assay showed concentration-dependent antioxidant activity, reaching 79.00 ± 0.50% RSA at 5 mg, with an estimated IC_{50} of ~2.17 mg. The findings establish BAE-CuPNHs as plant-mediated copper phosphate nanohybrids with substantial phytochemical immobilization and retained antioxidant functionality, providing a promising platform for further investigation in antioxidant-related applications.

ACKNOWLEDGEMENTS

One of the authors, Rutuja Palaskar gratefully acknowledges Chhatrapati Shahu Maharaj Research, Training and Human Development Institute (SARTHI), Pune, India for fellowship & Department of Microbiology, Savitribai Phule Pune University (SPPU), Pune, India for providing the required facilities.

CONFLICT OF INTEREST

The authors declare that there is no conflict of interests regarding the publication of this article.

DECLARATION OF AI-ASSISTED TECHNOLOGIES

During the preparation of this manuscript, the authors used an AI-assisted tool(s) to improve the language and no data, results or scientific conclusions were generated by AI. All analyses, interpretations and conclusions are the authors' own. The authors reviewed and edited the content and take full responsibility for the published work.

REFERENCES

1. P. Sachan, P. Shrivastava, A. Kushwaha, K. Jain and L. Kant, *J. Integr. Anatolian Med.*, **6**, 40 (2025); https://doi.org/10.53445/batd.1581503
2. D. Abeysinghe, K.K. Kumara, K.A.G. Kaushalya, U.G. Chandrika and D.D.S. Alwis, *Heliyon*, **7**, e07449 (2021); https://doi.org/10.1016/j.heliyon.2021.e07449
3. S. Gangaram, Y. Naidoo, Y.H. Dewir and S. El-Hendawy, *Plants*, **11**, 82 (2021); https://doi.org/10.3390/plants11010082
4. S. Singh, M. Kumar, S. Dwivedi, A. Yadav and S. Sharma, *Front. Plant Sci.*, **13**, 1076871 (2023); https://doi.org/10.3389/fpls.2022.1076871
5. W. Sudheer and N. Praveen, *Plant Sci. Today*, **8**, 491 (2021); https://doi.org/10.14719/pst.2021.8.3.1117
6. H. Omidian, A. Akhzarmehr and C.D. Bertol, *Int. J. Cosmet. Sci.*, **48**, 394 (2025); https://doi.org/10.1111/ics.70039
7. D. Xu, Y. Li, X. Meng, T. Zhou, Y. Zhou, J. Zheng, J. Zhang and H. Li, *Int. J. Mol. Sci.*, **18**, 96 (2017); https://doi.org/10.3390/ijms18010096
8. A. Vaiserman, A. Koliada, A. Zayachkivska and O. Lushchak, *Front. Bioeng. Biotechnol.*, **7**, 447 (2020); https://doi.org/10.3389/fbioe.2019.00447
9. U. Koca-Caliskan, C. Donmez, N. Eruygur, F. Ayaz, C. Altinkaynak and N. Ozdemir, *Chem. Biodivers.*, **19**, e202200476 (2022); https://doi.org/10.1002/cbdv.202200476
10. F.P. da Costa, E.P. Cipolatti, A. Furigo Jr. and R. Oliveira Henriques, *Chem. Rec.*, **22**, e202100293 (2022); https://doi.org/10.1002/tcr.202100293
11. J. Ge, J. Lei and R.N. Zare, *Nat. Nanotechnol.*, **7**, 428 (2012); https://doi.org/10.1038/nnano.2012.80
12. N. Özdemir, C. Altinkaynak, M. Türk, F. Geçili and S. Tavlaşoğlu, *Polym. Bull.*, **79**, 9697 (2022); https://doi.org/10.1007/s00289-021-03973-7
13. E. Bor, U. Koca Caliskan, C. Anlas, G.D. Durbilmez, T. Bakirel and N. Ozdemir, *Inorg. Nano-Met.Chem.*, **54**, 570 (2024); https://doi.org/10.1080/24701556.2022.2072342
14. F. Koca, H. Muhy, M. Halıcı, B. Gozcelioglu and B. Konuklugil, *Appl. Nanosci.*, **13**, 4787 (2023); https://doi.org/10.1007/s13204-022-02618-z
15. B. Somtürk-Yilmaz, *J. Inorg. Organomet. Polym. Mater.*, **34**, 5329 (2024); https://doi.org/10.1007/s10904-024-03169-2
16. M. Garcia-Vaquero, V. Ummat, B.K. Tiwari and G. Rajauria, *Marine Drugs*, **18**, 172 (2020); https://doi.org/10.3390/md18030172
17. K. Pusty, K. Kumar Dash, S. Giri, G.V.S.B. Raj, A. Tiwari, A.M. Shaikh and K. Béla, *Ultrason. Sonochem.*, **102**, 106762 (2024); https://doi.org/10.1016/j.ultsonch.2024.106762
18. A. Antonio-Pérez, L. Durán-Armenta, M. Pérez-Loredo and A. Torres-Huerta, *Micromachines*, **14**, 1882 (2023); https://doi.org/10.3390/mi14101882
19. K. Wolfe, X. Wu and R.H. Liu, *J. Agric. Food Chem.*, **51**, 609 (2003); https://doi.org/10.1021/jf020782a
20. C. Chang, M. Yang, H. Wen and J. Chern, *J. Food Drug Anal.*, **10**, (2020); https://doi.org/10.38212/2224-6614.2748
21. S. Baliyan, R. Mukherjee, A. Priyadarshini, A. Vibhuti, A. Gupta, R. Pandey and C. Chang, *Molecules*, **27**, 1326 (2022); https://doi.org/10.3390/molecules27041326
22. I. Gulcin and S. Alwasel, *Processes*, **11**, 2248 (2023); https://doi.org/10.3390/pr11082248
23. S. Bhapkar, U. Choudhari, U. Jadhav and S. Jagtap, *Sensors Int.*, **4**, 100242 (2023); https://doi.org/10.1016/j.sintl.2023.100242
24. G. He, W. Hu and C. Li, *Colloids Surf. B Biointerfaces*, **135**, 613 (2015); https://doi.org/10.1016/j.colsurfb.2015.08.030
25. S.S. Chandel, M. Salim and I.P. Kumhar, *Int. J. Adv. Acad. Stud.*, **5**, 20 (2023); https://doi.org/10.33545/27068919.2023.v5.i3a.947
26. S. Pai, P. Kshirsagar, N. Pawar and M. Nimbalkar, *Pharmacogn. Mag.*, **18**, 80 (2022); https://doi.org/10.4103/pm.pm_77_22
27. I. Solaberrieta, C. Mellinas, A. Jiménez and M.D. Garrigós, *Foods*, **11**, 3068 (2022); https://doi.org/10.3390/foods11193068

28. H. Kaur, N. Bari, A. Garg and S. Sinha, *Int. J. Biol. Macromol.*, **176**, 106 (2021); https://doi.org/10.1016/j.ijbiomac.2021.01.217
29. J. Xu, J. Wang, J. Ye, J. Jiao, Z. Liu, C. Zhao, B. Li and Y. Fu, *Adv. Sci.*, **8**, 2101101 (2021); https://doi.org/10.1002/advs.202101101
30. K. Bobrowska, K. Sadowska, K. Stolarczyk, M. Prześniak-Welenc, P. Golec and R. Bilewicz, *Int. J. Nanomedicine*, **18**, 6449 (2023); https://doi.org/10.2147/IJN.S427258
31. Ç. Sinmez and F. Koca, *J. Biol. Eng.*, **19**, 1 (2025); https://doi.org/10.1186/s13036-024-00464-x
32. S. Yusufbeyoglu, M. Yuruk, I. Ocsoy and A. Baldemir Kilic, *ChemistrySelect*, **11**, e202502863 (2026); https://doi.org/10.1002/slct.202502863
33. R. Pol, A. Rahaman, M. Diwakar, A. Pable, S. Jagtap, V.T. Barvkar and U.U. Jadhav, *Environ. Sci. Pollut. Res. Int.*, **31**, 38723 (2023); https://doi.org/10.1007/s11356-023-28735-y
34. A. Baldemir Kılıç, N. Ildız, S. Yusufbeyoğlu and İ. Öçsoy, *Inorg. Nano-Met. Chem.*, **55**, 18 (2025); https://doi.org/10.1080/24701556.2023.2240757